Peer-reviewed version available at Int. J. Mol. Sci. 2018, 19, 2053; doi:10.3390/ijms19072053

Article

Engineering cell adhesion and orientation via ultrafast laser fabricated microstructured substrates

Eleftheria Babaliari[1,2], Paraskevi Kavatzikidou[1], Despoina Angelaki[1,3], Lefki Chaniotaki[2], Alexandra Manousaki[1], Alexandra Siakouli-Galanopoulou[4], Anthi Ranella[1,*] and Emmanuel Stratakis[1,2,*]

[1]Foundation for Research and Technology - Hellas (F.O.R.T.H.), Institute of Electronic Structure and Laser (I.E.S.L.); ebabaliari@iesl.forth.gr; ekavatzi@iesl.forth.gr; despoinaangelaki@gmail.com; ranthi@iesl.forth.gr; stratak@iesl.forth.gr

[2] Department of Materials Science and Technology, University of Crete, Crete, Greece; ebabaliari@iesl.forth.gr; mst1095@edu.materials.uoc.gr; stratak@iesl.forth.gr

[3] Department of Physics, University of Crete, Crete, Greece; despoinaangelaki@gmail.com

[4] Department of Biology, University of Crete, Crete, Greece; siakouli@biology.uoc.gr

* Correspondence: stratak@iesl.forth.gr; Tel.: +30 2810 391274

Abstract: Cells take decisions on their responses depending on the stimuli received by the surrounding extracellular environment, that provides the essential cues at the micro and the nano-lengthscales required for adhesion, orientation, proliferation and differentiation. In this study, discontinuous microcones on silicon (Si) and continuous microgrooves on polyethylene terephthalate (PET) substrates were fabricated via ultrashort-pulsed laser irradiation at various fluences, resulting in microstructures with different roughness and geometrical characteristics. The topographical models attained were specifically developed to imitate the guidance and alignment of Schwann cells for oriented axonal regrowth, towards nerve regeneration. At the same time, positive replicas of the silicon microstructures formed were successfully reproduced, via soft lithography, on the biodegradable polymer poly(lactide-co-glycolide) (PLGA). The anisotropic continuous (PET) and discontinuous (PLGA replicas) microstructured polymeric substrates were assessed in terms of their influence on the Schwann cells responses. It is shown that the developed micropatterned substrates enable control over the cellular adhesion, proliferation and orientation and are thus useful to engineer cell alignment *in vitro*. This property could be potentially useful in the fields of neural tissue engineering and for dynamic microenvironment systems that simulate *in vivo* conditions.

Keywords: Cell adhesion, cell orientation, Schwann cells, topography, laser fabrication, soft lithography, polymeric materials

1. Introduction

Cell behavior *in vivo* is influenced by a variety of extracellular signals. It is currently clear that many cellular aspects, including adhesion, migration, spreading, proliferation, survival, apoptosis and gene expression, are modulated by interdependent signaling cascades of soluble signals, shear stresses, other supportive cells and the nature of the extracellular matrix (ECM) [1]. Thus, the main challenge and goal of tissue engineering is to mimic the features of the ECM and the surrounding environment of cells sufficiently so that cells will function in the artificial medium as they would *in vivo* [2]. Furthermore, individual cells recognize structures that have comparable dimension to the cellular size, which is at the micro-scale. Consequently, control over micro/nano-topography is desirable. At the cell-material interface, all the cellular processes are governed by the physical and chemical stimuli of substrate stiffness (or rigidity), topography and chemistry respectively; while at

the intracellular level, focal adhesions are key molecular complexes for sensing the environmental conditions as significant mechanosensitive players [3–6]. Indeed, many studies confirmed that the surface topography influences the adhesion, migration, polarization, proliferation, and differentiation of cells [7–12]. These parameters are of high significance for the design and development of advanced biomaterials in regenerative medicine and tissue engineering. Therefore, a considerable amount of research devoted to the modification of materials' surfaces to use them as platforms to study cell viability, differentiation, motility, and apoptosis [13,14].

Generally, there are various materials and fabrication techniques that aim to re-construct *in vitro* the ECM architecture with very specific compositions, ligand presentations, mechanical properties, and organization that vary between different tissues [13–15]. Indeed, previous studies have been shown in detail the major fabrication techniques, the produced types of micro/nanostructured substrates and advantages/disadvantages of the techniques [16,17]. Among various techniques that have been developed for surface modification, laser irradiation has proved to be important in the enhancement of materials biocompatibility, particularly via the creation of new functional groups and the precise topography formation at the cellular and sub-cellular scale [10,18–21]. Microstructuring via ultrafast lasers in particular, provides unique control over the uniformity and regularity of micron and submicron features [22].

Guiding neurite outgrowth *in vitro* is important in tissue regeneration and for the development of neuronal interfaces with advantageous characteristics. To date, this has been achieved with micro- and nano-fabrication techniques giving rise to various anisotropic continuous or discontinuous geometries [13,14]. Previous studies have been demonstrated that anisotropic continuous electrospun polymeric fibers could influence neurite growth, alignment and differentiation [23–25]. It has been also shown that in photolithographically fabricated continuous grooved substrates axons were grown on top of the ridges [25–27]. Moreover, it has been profoundly presented the impact of the disordered/anisotropic nanotopographical features on neuron differentiation and maturation by mechanotranductive pathways in PC12 cells [28–30]. It has also been reported that the laser microstructured discontinuous Si substrates not only support the cellular adhesion and viability but also significantly affect cells morphology, growth, orientation and differentiation in a surface-dependent manner [10,20,21]. Furthermore, it has been presented that both Schwann cells and axons of sympathetic neurons were parallel oriented onto microcone patterns of elliptical cross-section, while they exhibited a random orientation onto the microcones exhibiting arbitrarily-shaped cross-sections. As a result, it is suggested that an anisotropic continuous and discontinuous topographical pattern could promote Schwann cell and axonal alignment, provided that it hosts anisotropic geometrical features, even though the sizes of those range at the subcellular length scale [20]. The same topographical model also has been used to study the PC12 differentiation after treatment with NGF. It was shown that, unlike low and medium roughness surfaces, highly rough ones exhibiting large distances between microcones did not support PC12 cell differentiation, although cells had been stimulated with NGF [21]. Such substrates were also shown to support the macrophage adherence and the antigen presentation process *in vitro*, and to induce the specific antibody production upon implantation *in vivo* [31].

Soft lithography is used to produce substrates with distinct surface topographies at the nano- and micro-meter scale**.** It has been successfully used to transfer well-defined micro-sized patterns from silicon or stainless steel masters to surfaces of soft biomaterials [32,33] allowing the recreation of controlled microenvironments and an in-depth study of the influence of surface properties on cell behavior [34].

As aforementioned in our previous studies, we have already well characterized discontinuous Si surfaces as cell substrates and we have extensively investigated specific cell responses of various neuronal cell types on them. In this study, we aim to demonstrate the reproducibility (or not) of Schwann cell behavior, focusing on growth, adhesion and orientation, on laser patterned polymeric

microstructures, including PET and PLGA compared with the Si substrates. PET has been widely used for cell culturing, surgical suture material and prosthetic vascular grafts due to its biocompatibility and its excellent mechanical strength and resistance [35,36]. Moreover, PLGA is a biodegradable synthetic polymer featured as biocompatible and is used in various microfabrication techniques to create patterned substrates for various applications in Tissue Engineering and Regenerative Medicine [37–40]. In particular, microstructured substrates of different continuous microgrooves (MG) and discontinuous microspikes (MS) topographies were fabricated via either ultrafast laser direct writing of 2D planar PET substrates [41], or through soft lithography of PLGA replicas from micro-structured Si substrates respectively. The morphological, topographical, wetting and optical properties of these substrates were investigated and then their interactions with Schwann cells (SW10), a murine glia cell line, in terms of adhesion, orientation and proliferation were determined.

2. Results and Discussion

2.1 Scanning Electron Microscopy (SEM) images of laser-microstructured substrates on PET (PET-MG) and PLGA-MS (1:10) replicas (from laser-microstructured Si substrates with three different laser fluences)

Figure 1a depicts the SEM images of PET coverslips that were ablated by the femtosecond laser at a constant fluence of 11.9 J/cm^2, scan velocity of 7 mm/s and a x_{step} (distance between two consecutive scan lines) of 50 μm fabricated using the linear Gaussian beam. Thus, using these parameters, we fabricated microstructured substrates with the geometry of continuous microgrooves (PET-MG substrates). Such surface morphology occurs due to the overlap between adjacent spots during the scanning process [42]. Figures 1b and c respectively represent the different stages of the soft lithography process; from the Si master with microspikes through PDMS negative mold to the PLGA replicas of the three different topographies (Si-MS and PLGA-MS replicas). We have successfully reproduced (irradiated Si topography and PLGA replicas) patterned substrates exhibiting 2D-3D surface characteristics, resulting in an additional parameter to control cell growth and network formation. As shown in Figure 1c, each culture substrate consisted of these three microstructured areas, irradiated using 0.42 J/cm^2 (25mW-low roughness), 0.58 J/cm^2 (40mW-medium roughness) and 0.72 J/cm^2 (65mW-high roughness). The main difference of the three PLGA-MS replicas is focused on the distance between the spikes thus spikes size (aspect ratio). The higher the laser fluence the higher the spike size, characterized as high roughness or topography.

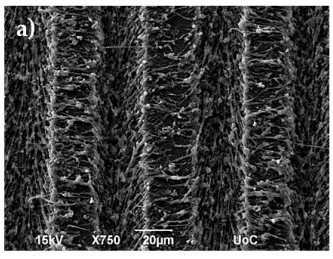

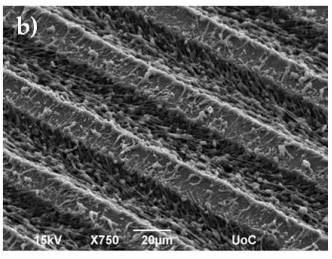

PET-MG substrate	
Width (w) (μm)	28.68 ± 0.47
Depth (d) (μm)	8.87 ± 0.44
Aspect ratio (A)	0.309
Roughness ratio (r)	1.62
Contact angle (°)	108.2

Figure 1a. Scanning Electron Microscopy (SEM) images [top (a) and tilted (b) view] of PET-MG substrates. Measurements of the geometrical parameters of the surface of the PET-MG substrates on the tilted view of SEM images were processed by Fiji ImageJ. A series of measurements were obtained for the surface characterization such as width (w) and depth (d) of microgrooves, aspect ratio (A = d/w) and roughness ratio (r = 1 + 2d/w). Measurements of the contact angles were performed with the use of a tensiometer.

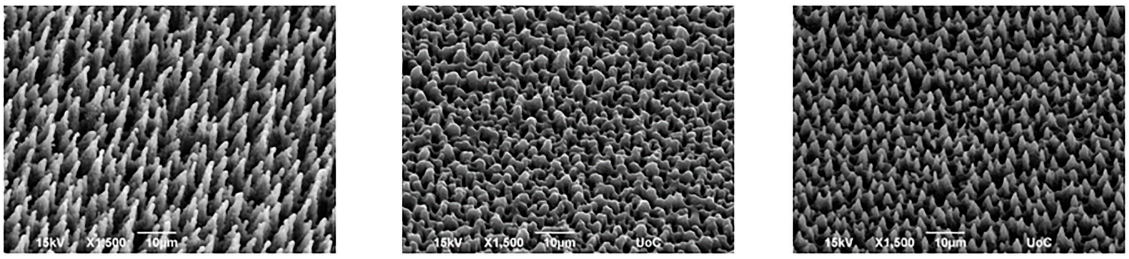

Si master, High roughness-topography, Laser Fluence 0.72 J/cm²

PDMS Negative mold

PLGA-MS replica

Figure 1b. Scanning Electron Microscopy (SEM) images (tilted view) of a laser-microstructured Si-MS substrate (High roughness-topography)-mold, PDMS Negative mold and PLGA-MS replica.

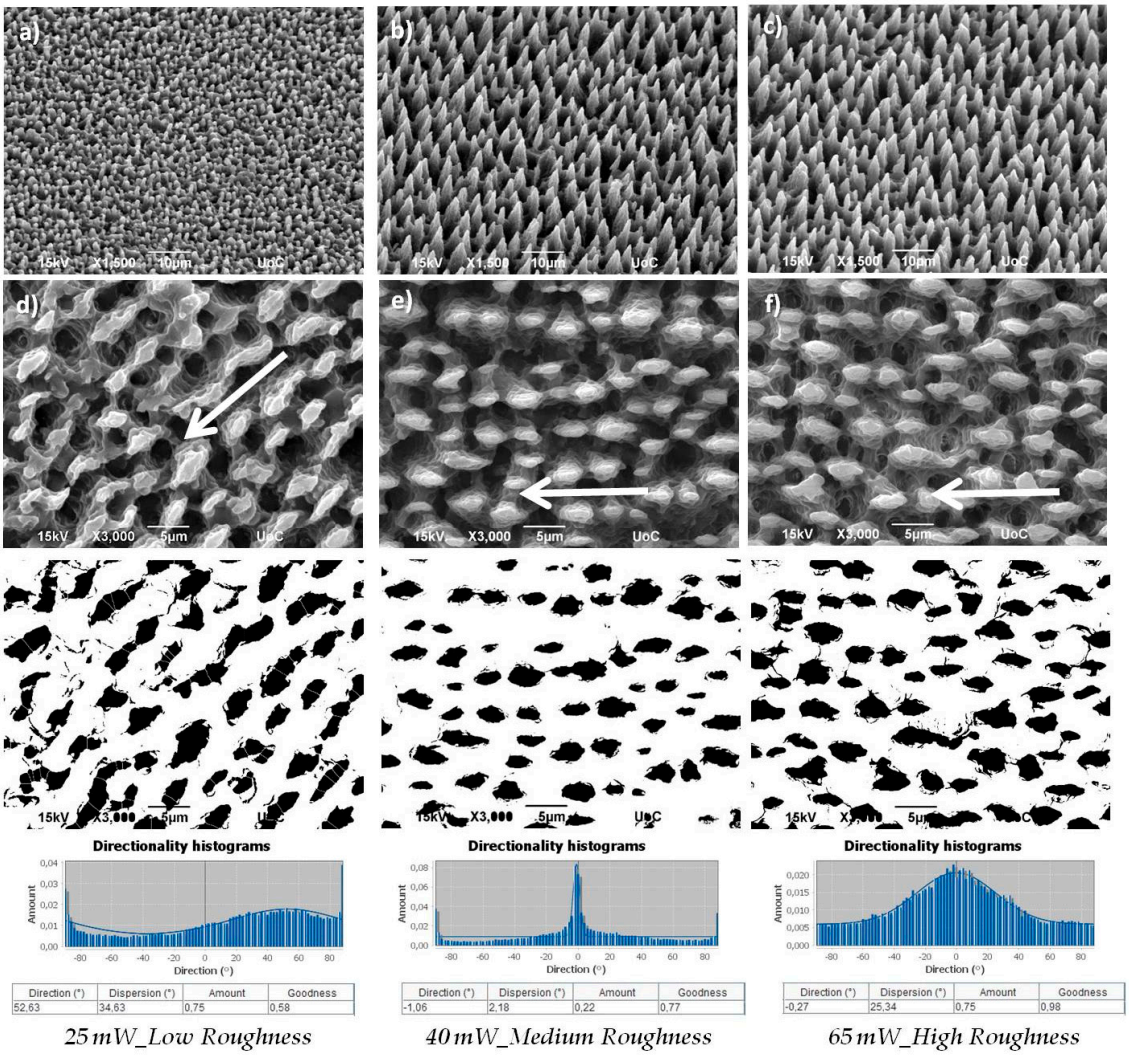

25 mW_Low Roughness

40 mW_Medium Roughness

65 mW_High Roughness

Groups PLGA-MS	Density [10(4) / mm(2)]	Height (h) (μm)	Width (b) (μm)	Aspect ratio (A)	Roughness ratio (r)	Contact Angle (°)
25mW_Low Roughness	7.18 ± 1.30	3.06 ± 0.40	2.93 ± 0.30	1.044	3.1	120
40mW_Medium Roughness	5.35 ± 0.25	4.34 ± 0.36	2.16 ± 0.31	2.005	5.0	124
65mW_High Roughness	4.69 ± 0.19	10.55 ± 1.10	4.68 ± 0.41	2.252	5.5	133

Figure 1c. Scanning Electron Microscopy (SEM) images [tilted (a, b, c) and top (d, e, f) view] of PLGA-MS replicas of the three different topographies (25 mW_Low Roughness, 40 mW_Medium Roughness and 65 mW_High Roughness). Under images the directionality histograms and the tables with the statistics generated are presented using the Fiji ImageJ plug-in "Directionality" [43]. On top of the histogram, the plug-in tries to generate statistics on the highest peak found. The highest peak is fitted by a Gaussian function, taking into account the periodic nature of the histogram. At the tables, the "Direction (°)" column reports the center of the Gaussian; the "Dispersion (°)" column reports the standard deviation of the Gaussian; the "Amount" column is the sum of the histogram from center-std to center+std, divided by the total sum of the histogram; the "Goodness" column reports the goodness of the fit where 1 is good, 0 is bad. Measurements of the geometrical parameters of the surface of the PLGA-MS (10%) replicas at the three different topographies (25mW_Low Roughness, 40 mW_Medium Roughness and 65mW_High Roughness) on the SEM images (top and tilted view) of the PLGA-MS replicas were processed. In particular an image-processing algorithm (Fiji ImageJ) was implemented in order to determine the topological characteristics of the MSs, including height (h), width (d), aspect ratio (A) and roughness ratio (r) from top (highest magnification), and tilted-view SEM images. The aspect ratio was calculated by dividing the height by the radius of the spike's base. In the case of the PLGA-MS replicas, a surface plot of each image was produced by Fiji ImageJ, and the height and spike's base were measured. From each image at least 10 measurements were performed. The roughness ratio, r, was calculated by dividing the actual, unfolded, surface area of spikes by the total irradiated area ($r = 1 + 2h/b$, where b is the width of spikes). The mean value was calculated from statistics performed at 4 individual surfaces in each case. Measurements of the contact angles were performed with the use of a tensiometer.

The measurements of the geometrical parameters of the PET-MG substrates, as calculated from SEM images, are summarized in Figure 1a. It was found that the width of the microgrooves was (28.68 ± 0.47) μm, the depth (8.87 ± 0.44) μm, the aspect ratio 0.309 and the roughness ratio 1.62. The geometrical characteristics of the spikes on the Si substrates have been already determined [20,21]. Here, in Figure 1c, we also show the measurements of the geometrical parameters of the surface of the PLGA-MS replicas at the three different topographies. As calculated from SEM images, the spike height varied from (3.06 ± 0.40) μm in the low-roughness structures to (10.55 ± 1.10) μm in the high-roughness structures (Figure 1c). While spike density was the lowest in the high-roughness structures, the spikes' height and roughness, thus aspect ratio increased. These findings demonstrate the anisotropic nature of the PLGA-MS substrates. Furthermore, it is clear from Figure 1c, and specifically from the directionality histograms, that there is a varied orientation between the replicas. The medium and high roughness PLGA-MS substrates showed a directionality at the area of zero degrees, while the low roughness showed a lower directionality at the area close to 52 degrees.

2.2 Measurements of wettability of irradiated PET (PET-MG), non-irradiated PET (PET-Flat) and PLGA-MS (1:10) replicas (from irradiated Si substrates)

The contact angle measured on the irradiated PET (PET-MG substrate) is presented in Figure 1a. Specifically, the contact angle of the non-irradiated PET (PET-Flat) was ~77.8°, which was in agreement with previous studies [35,44], while the contact angle of the irradiated (PET-MG) was 108.2°. We observed a decrease in the hydrophilicity of PET-MG substrate which is attributed to the increased roughness of the surfaces after irradiation with the femtosecond laser [45]. Figure 1c shows the measured contact angles of PLGA-MS (1:10) replicas of the three topographies. By

increasing the roughness of the PLGA-MS replica's surface, the hydrophilicity was decreased. According to the literature, lactide is more hydrophobic than glycolide, therefore PLGA copolymers rich in lactide (the PLGA in this study) are less hydrophilic and absorb less water, leading to a slower degradation of the polymer chains [46]. Therefore the topography enhances the degradation rate of this PLGA copolymer.

2.3 UV-Vis measurements of irradiated PET (PET-MG), non-irradiated PET (PET-Flat) and PLGA-MS (1:10) replicas (from irradiated Si substrates)

In order to determine any changes on the surface chemistry of the microstructured substrates, the spectroscopy of ultraviolet-visible (UV-Vis) has been used. We observed an increase of the absorption in the irradiated PET (PET-MG) due to the structuring process. Moreover, we noticed a development of an absorption band, in the region of 300–500 nm, in PET-MG , probably due to the presence of aromatic hydroxylated species produced during the photooxidation of PET (Figure 2a), which was in agreement with previous studies [47–49]. Specifically, previous work [47–49] has demonstrated the development of an absorption band, around 340 nm, in the UV range. The relevant absorbance (a.u.) exhibits an increase in the PLGA topographies compared with the flat PLGA and the glass substrate as shown in Figure 2b. By increasing the topography or laser fluence of the PLGA-MS replicas, the absorbance was increased (A_25<A_40<A_65mW). All absorption bands (obtained here by UV-Vis and unpublished data by ATR-FTIR on these replicas) found in the spectra agree with those given in the literature for PLGA copolymers [46,50]. It was observed that there was a slight difference in the relevant absorbance of the microstructured replicas compared with the flat PLGA but it was negligible.

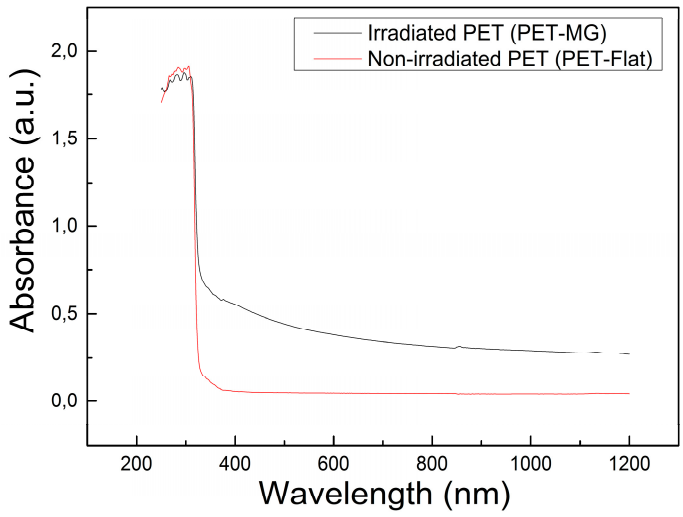

Figure 2a. UV-Vis measurements of irradiated PET (PET-MG) and non-irradiated PET (PET-Flat).

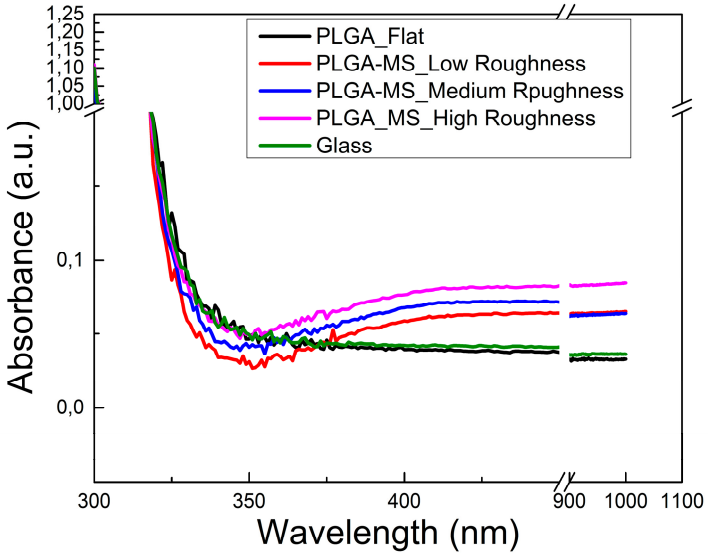

205

206 **Figure 2b.** UV-Vis measurements of all the PLGA-MS replicas as well as PLGA flat and glass substrate.

207

208 **2.4 Cell seeding of laser-microstructured substrates on PET (PET-MG) and PLGA-MS replicas**
209 **with Schwann cells**

210 In Figure 3a, we show the morphology of Schwann cells for two different time points (four days and
211 six days) cultured on the PET substrates (PET-MG and PET-Flat). The anisotropic continuous
212 microgrooves had a width of (28.68 ± 0.47) μm and a depth of (8.87 ± 0.44) μm. We noticed that the
213 cells exhibited a branched shape and flattened morphology with long cellular extensions that signal
214 good adhesion and growth of the cells on the microgrooves. Moreover, we noticed that the cells
215 appeared to be oriented along the direction of the microgrooves for four and six days of culture
216 while they showed a random orientation on the flat PET. This is also demonstrated by the
217 directionality histograms in Figure 3a which show that the amount is higher in the domain parallel
218 to the microgrooves (±90 degrees). It is obvious, from the SEM images in Figure 3a, that although
219 surface roughness did not affect the proliferation of the cells (cells were equally grown on flat PET
220 and PET-MG substrates) surface morphology significantly controlled the outgrowth of the cells.
221 Consequently, cells could sense continuous directional topographical cues with sizes ranging at the
222 subcellular length scale.

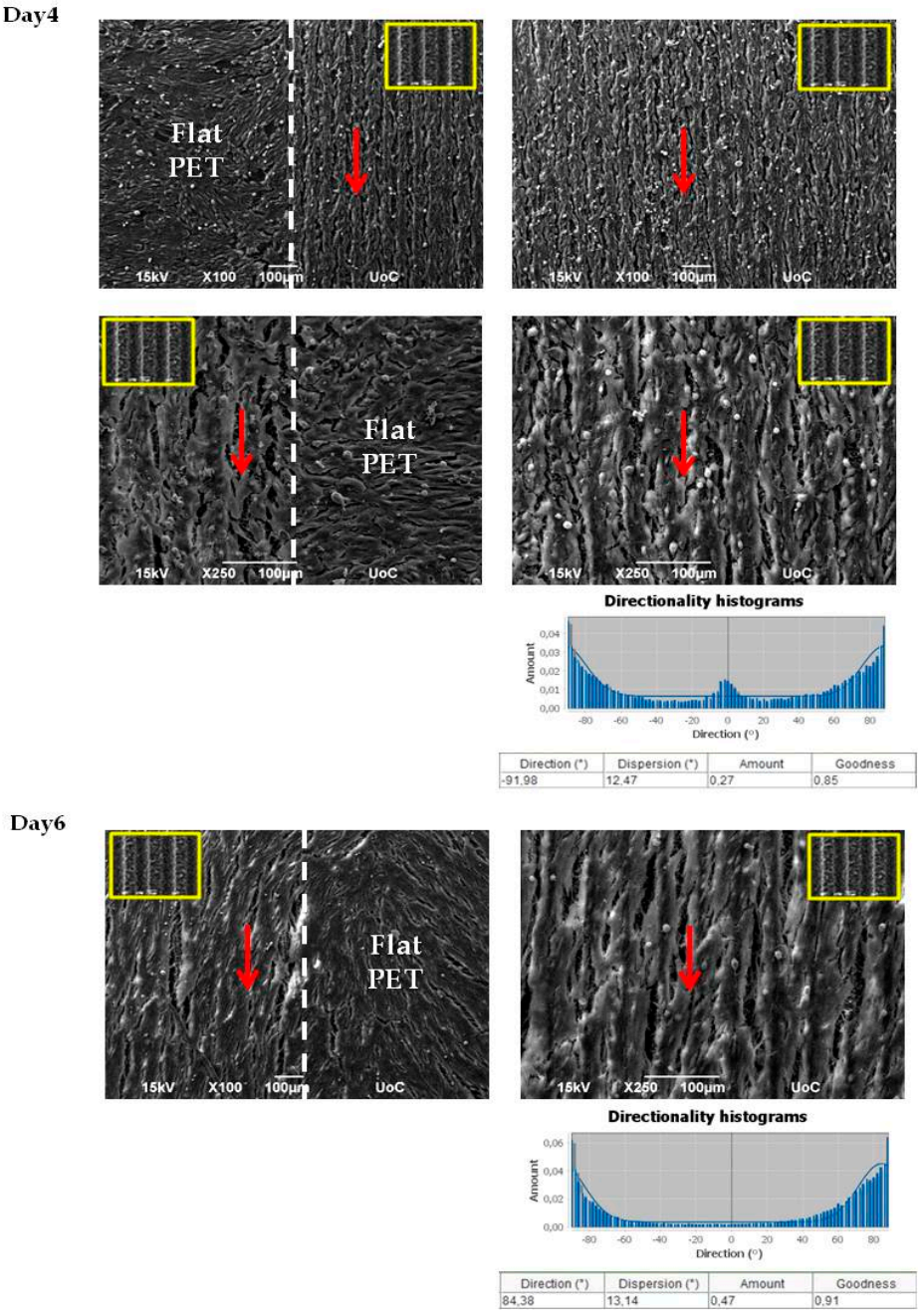

Figure 3a. Scanning Electron Microscopy (SEM) images of Schwann cells cultured on the PET substrates (PET-MG and PET-Flat) for four and six days. The red arrows represent the directionality of Schwann cells according to the direction of the microgrooves. The inset SEM images, indicated by the yellow box, show the geometry of microgrooves. Under SEM images the directionality histograms and the tables with the statistics generated are presented using the Fiji ImageJ plug-in "Directionality" [43]. On top of the histogram, the plug-in tries to generate statistics on the highest peak found. The highest peak is fitted by a Gaussian function, taking into account the periodic nature of the histogram. At the tables, the "Direction (°)" column reports the center of the Gaussian; the "Dispersion (°)" column reports the standard deviation of the Gaussian; the "Amount" column is the sum of the histogram from center-std to center+std, divided by the total sum of the histogram; the "Goodness" column reports the goodness of the fit where 1 is good, 0 is bad.

Preprints (www.preprints.org) | NOT PEER-REVIEWED | Posted: 25 June 2018 doi:10.20944/preprints201806.0380.v1

Peer-reviewed version available at Int. J. Mol. Sci. 2018, 19, 2053; doi:10.3390/ijms19072053

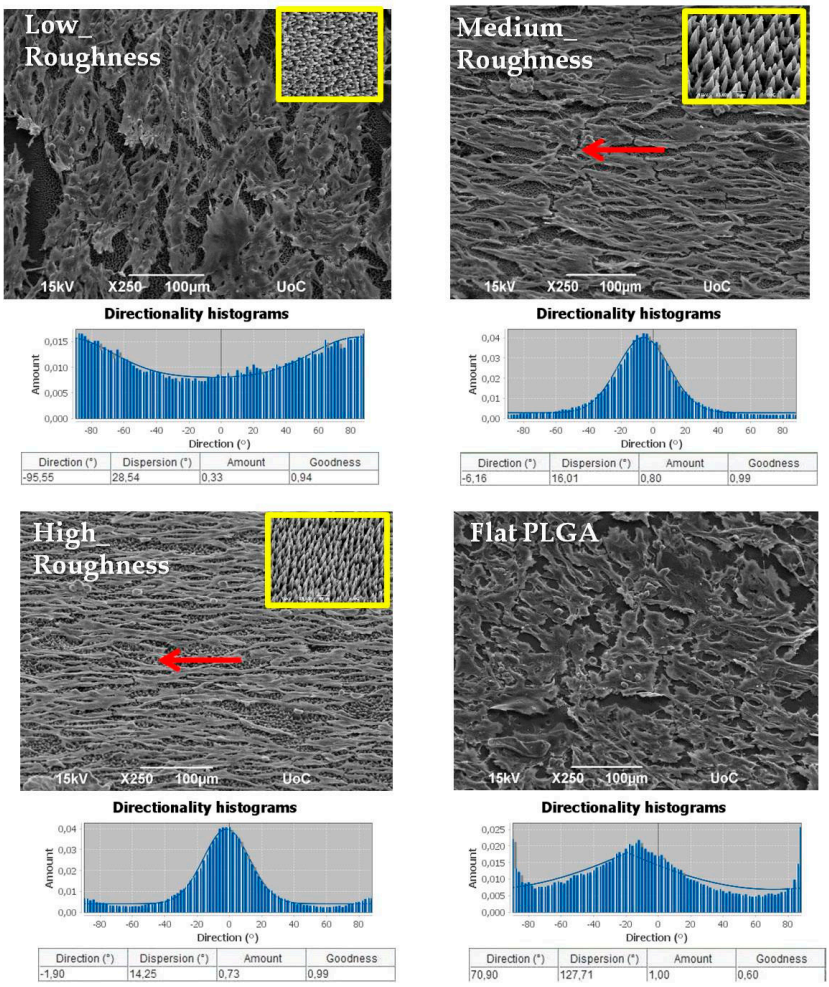

Figure 3b. Scanning Electron Microscopy (SEM) images of Schwann cells cultured on the PLGA-MS replicas (three topographies) and on flat PLGA for three days. The red arrows represent the directionality of Schwann cells according to the topography of the PLGA-MS replica (inset SEM image, indicated by the yellow box, on the right side of each group). Under SEM images the directionality histograms and the tables with the statistics generated are presented using the Fiji ImageJ plug-in "Directionality" [43]. On top of the histogram, the plug-in tries to generate statistics on the highest peak found. The highest peak is fitted by a Gaussian function, taking into account the periodic nature of the histogram. At the tables, the "Direction (°)" column reports the center of the Gaussian; the "Dispersion (°)" column reports the standard deviation of the Gaussian; the "Amount" column is the sum of the histogram from center-std to center+std, divided by the total sum of the histogram; the "Goodness" column reports the goodness of the fit where 1 is good, 0 is bad.

According to Figure 3b, there is the apparent finding that all three discontinuous topographies on the PLGA-MS replicas equally support Schwann cells' growth. It is demonstrated that there is a growth pattern/profile of the Schwann cells observed mainly on the medium and high roughness PLGA-MS replicas compared with the low PLGA-MS replica and flat PLGA substrate for three days of culture. The cells adhered and aligned on the ridge of the spikes of the medium and high topography. On the contrary, on the flat substrate and on the low PLGA-MS replica, there is an arbitrary cell growth occurring. The higher number of elongated cells are present on the high roughness and the medium roughness PLGA-MS replicas as demonstrated also from the directionality histograms, in Figure 3b, where the amount is clearly concentrated at the area of zero degrees compared to low roughness PLGA-MS replicas and flat PLGA. In this study, the topography (due to the laser irradiation process) of the polymeric substrates ranges in both the micro- and nano-scale. Our previous studies demonstrated that the adhesion, alignment, proliferation and differentiation of different types of neural cells depend on the topography [12-15]. Specifically, it has

been proved that there was a directional cell outgrowth dictated by the substrates of medium and high roughness[20]. In the present study, all the three topographies show cell growth according to the spikes' orientation (red arrows on Figure 3b) indicating that the cells could sense the discontinuous directional topographical features at subcellular lengthscales. To date, there are no widely accepted hypotheses regarding the mechanism for the effects of topography substrates on cell adhesion, orientation and proliferation. Moreover, a study demonstrated that in micro-grooved features, the ridge width is commonly larger than or equal to the size of a single cell, permissive for cell attachment and migration, as well as cell alignment following the geometrical guidance. In contrast, nano-grooved features are similar to the ECM architectures and are typically much smaller than a single cell, thus inducing cell alignment in a more fundamental way such as mimicking or signaling the cell membrane receptors [51].

2.5 Fluorescent images of Schwann cells seeded on laser-microstructured substrates on PET (PET-MG) (Immunostaining) and PLGA-MS replicas (Immunostaining)

In Figure 4, we present the fluorescent images of Schwann cells cultured on the PET substrates (PET-MG and PET-Flat) for four and six days. The actin filament of cytoskeleton is visualized with red color while the nuclei with blue color. We noticed that the cytoskeleton of the cells was elongated along the direction of the microgrooves whereas a random orientation observed on the flat PET. It is important to mention here that the width of the microgrooves is a critical parameter for the alignment of Schwann cells. The width of the Schwann cells ranges from (5-10) μm. It has been shown [14] that the pattern widths or spacings varying from (2-30) μm are optimal for the alignment of Schwann cells. Indeed, when we used a topography of microgrooves with a width of (28.68 ± 0.47) μm, cells appeared to be oriented along the direction of microgrooves (as it is shown in Figure 4) while when the width of the microgrooves was (168.12 ± 1.38) μm a random orientation of cells was observed (data not shown here). The findings of the PLGA-MS replicas seeded with Schwann cells exhibited the presence of elongated and round cells at a proliferation stage and signs of orientation according to the spikes (three days of culture). Specifically, Schwann cells grew more randomly and with an isotropic manner on low roughness PLGA-MS comparable with the flat PLGA. On medium and high roughness PLGA-MS replicas, the cells exhibited a directional growth. At the fifth day, the presence of elongated cells at different layers was shown and there was a full coverage of the surface. There was no difference between the three different topographies and the control substrate at this time period (Figure 5).

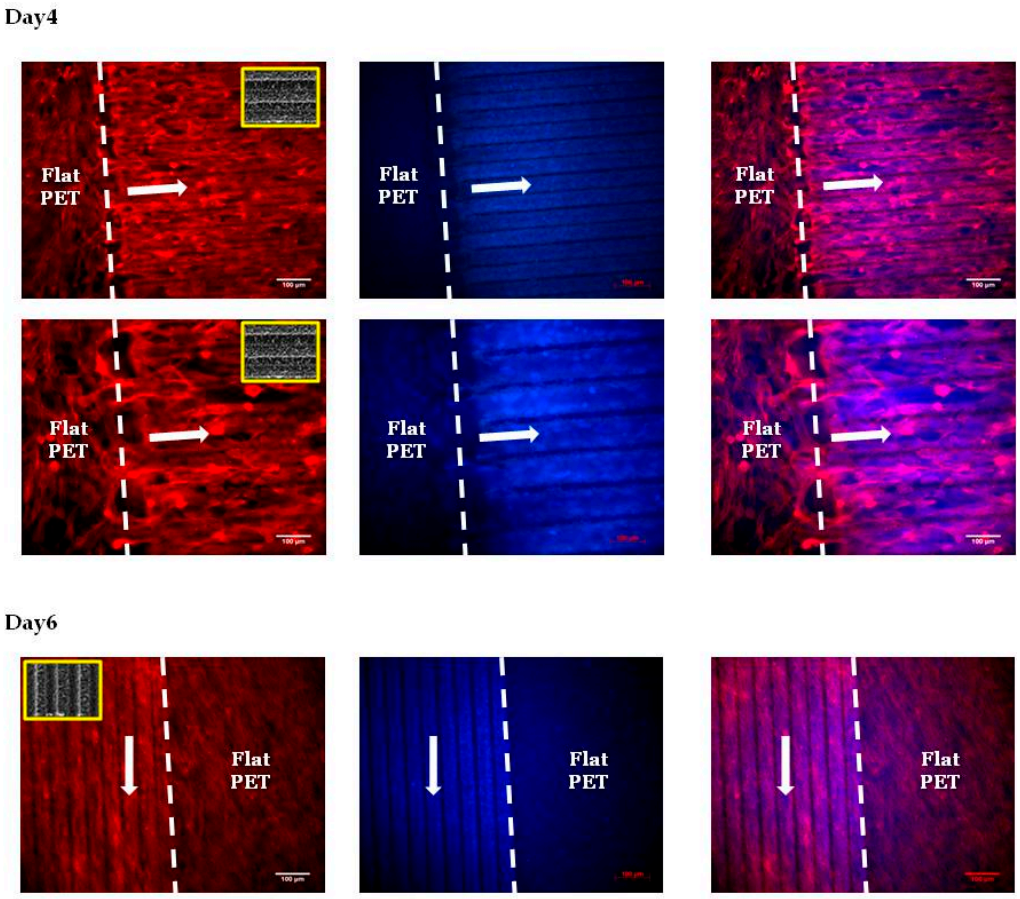

Figure 4. Fluorescent images of Schwann cells cultured on the PET substrates (PET-MG and PET-Flat) for four and six days. The cytoskeleton of the cells is visualized with red color (Alexa Fluor® 568 Phalloidin) while the nuclei with blue color (DAPI). The white arrows represent the directionality of Schwann cytoskeleton according to the direction of the microgrooves. The inset SEM images, indicated by the yellow box, show the geometry of microgrooves.

Preprints (www.preprints.org) | NOT PEER-REVIEWED | Posted: 25 June 2018 doi:10.20944/preprints201806.0380.v1

Peer-reviewed version available at Int. J. Mol. Sci. 2018, 19, 2053; doi:10.3390/ijms19072053

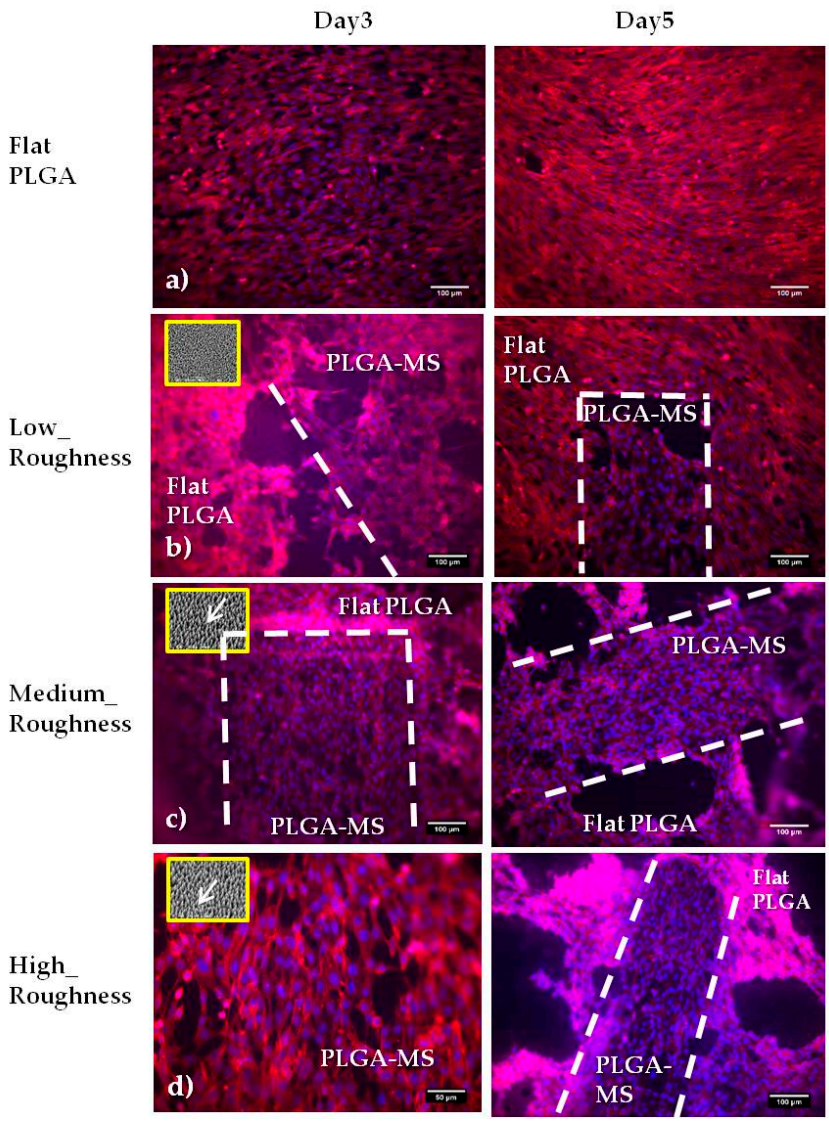

Figure 5. Fluorescent images of Schwann cells cultured on the (a) flat PLGA and PLGA-MS replicas (b, c and d) for three and five days. Each replica is defined by Low (b), Medium (c) and High (d) Roughness. The cytoskeleton of the cells is visualized with red color (Alexa Fluor® 568 Phalloidin). The white interrupted lines represent PLGA-MS area and thus spikes area. It should be noted here that for this specific study with the actin/DAPI assay, the PLGA-MS replicas (spike's area) was 0.3-0.5mm (width) and 1.5mm (length).The inset SEM images on the left side, indicated by the yellow box, show the topography of the PLGA-MS replicas and the white arrow represent the directionality of the spikes.

The outgrowth of Schwann cells (number of cells/mm^2) on the PET-MG substrate and on the flat PET was evaluated by counting cell nuclei stained with DAPI (Figure 4). Nuclei number was assessed with Fiji ImageJ analysis. Figure 6a depicts the mean cell number on the PET-MG substrate and flat PET for four and six days of culture. The cell outgrowth was improved on PET-MG substrate compared to the flat PET, in agreement with the SEM and fluorescent images, with a significant difference between four days and six days at PET-MG. According to Figure 6b, all three topographies on the PLGA-MS replicas support Schwann cells' growth (results that are confirmed from the SEM and fluorescent images too) and furthermore proliferation up to five days. The high

Peer-reviewed version available at Int. J. Mol. Sci. 2018, 19, 2053; doi:10.3390/ijms19072053

roughness PLGA-MS replicas report the highest cell number in both the time periods, followed by the medium roughness PLGA-MS replica; while the lowest cell proliferation is shown at the low roughness PLGA-MS replica. Taking into consideration Figures 5 and 6b, it is clear that these findings come in agreement with the previous work of our group on Si microstructured substrates where the surface roughness did not influence the Schwann cell growth, but the surface morphology (discontinuous pattern) played a key role for this response [20]. Schwann cells seemed to be aligned with the orientation of the spikes' topographical features and specifically this preference was more pronounced as the roughness increased. The key geometrical characteristics (height, width and aspect ratio) of the substrates leading to the anisotropic nature of the spikes and their parallel orientation varies between the three topographies and significantly affects the degree of cell alignment. The previous findings of the group are demonstrated in the present study too, with the cell growth on the low roughness substrates to have an isotropic manner such as flat and control materials (shown clearly here in Figure 5) and cell growth on medium and high roughness substrates exhibiting a more pronounced anisotropic manner (shown in Figures 3b and 5). It should be noted here that the height of the spikes and the interspike distance cannot be controlled by the microfabrication techniques used in this study, and since there is the step of replication of the topography from the Si master mold through PDMS negative mold finally to the PLGA-MS replica there is definitely a slight difference between the fabricated topography and the replicated topography in terms of the height of the spikes. These results demonstrate that the micro- and nano-structures favor the cell outgrowth.

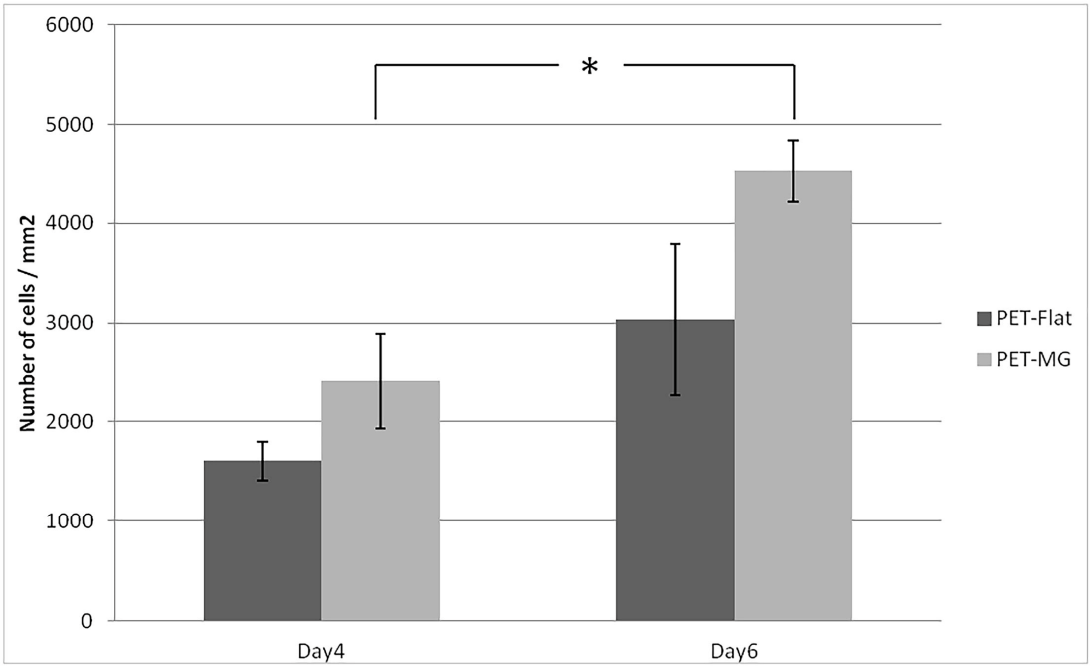

Figure 6a. Proliferation of Schwann cells (number of cells/mm^2) cultured on the PET substrates (PET-MG and PET-Flat) (via DAPI) for four and six days. The data were subjected to ANOVA with post-hoc Tukey HSD Test. A significant difference (*p<0.0.5) was observed between four days and six days at PET-MG substrate.

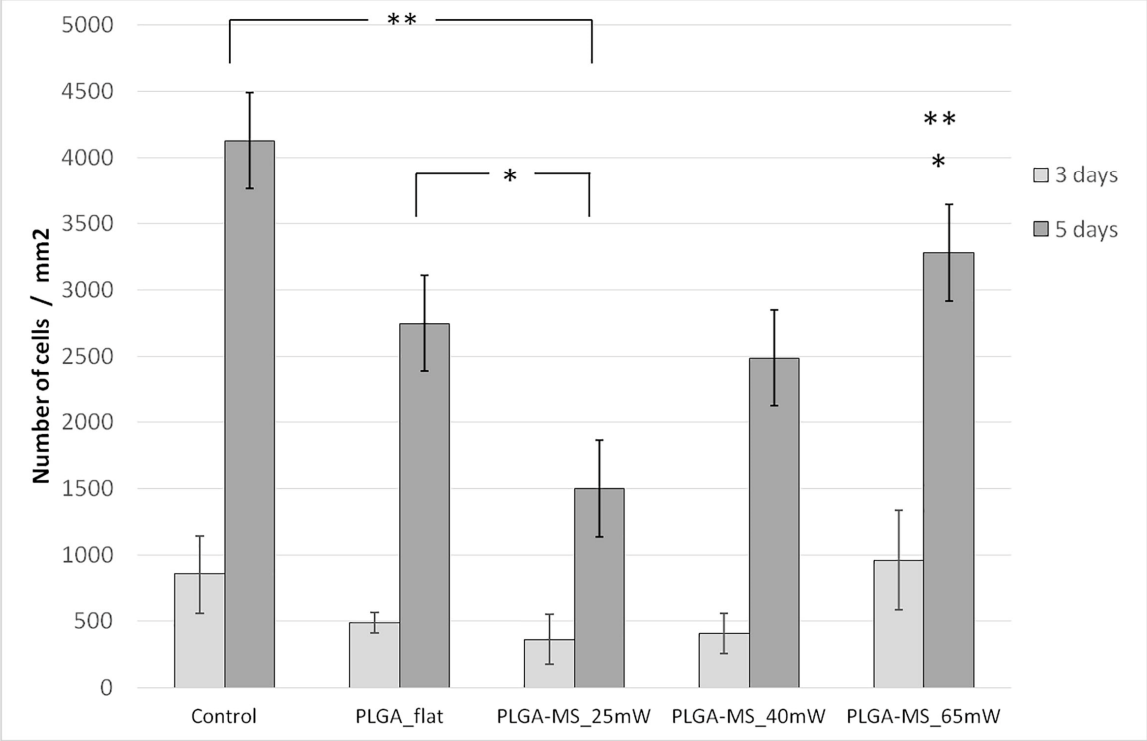

Figure 6b. Proliferation of Schwann cells (number of cells /mm^2) cultured on the PLGA-MS replicas, PLGA flat and control samples (via live dead assay, images not shown here) for three and five days. The data were subjected to ANOVA with post-hoc Tukey HSD Test for multiple comparisons between the groups. At three days, the p value > 0.05 and therefore the treatments (groups) are not significantly different for that level of significance. However at five days we observe some significantly differences strongly suggesting that one or more pairs of treatments (groups) are significantly different. In particular, the control group is significantly different to PLGA flat and PLGA-MS replicas of 25mW_Low Roughness and 65mW-High Roughness (**p<0.001); PLGA-MS replica 25mW_Low Roughness is significantly different to PLGA flat and replica 65mW-High Roughness (*p<0.05).

In this study, we demonstrated the efficacy of ultrafast-pulsed laser irradiation as a simple and effective method to fabricate micro- and nano-structures with controlled geometry and pattern regularity. Two different synthetic polymers, the fabricated PET-MG substrates and the produced PLGA-MS replicas at a range of laser fluences, resulting in different roughness and geometrical characteristics were investigated for their selective cellular adhesion, proliferation and orientation. In this context the effect of an anisotropic continuous and three anisotropic discontinuous topographies, on cellular response was studied.

The morphological characterization of the PET-MG substrates and the PLGA-MS replicas (SEM images) indicated a topography with microgrooves (anisotropic continuous) for the PET substrates and microspikes (anisotropic discontinuous) for the PLGA replicas. This is due to the different fabrication processes used; PET substrates were laser-irradiated directly, while the PLGA-MS replicas were produced by soft lithography of laser irradiated Si substrates. Thus, although the same laser irradiation process was used, the different materials formed a range of topographies, as shown in Figure 8. The composition and the mechanical properties of the material play a significant role in the topography [52]. The wetting and absorbance (related to optical properties) were assessed by the contact angle and the UV-Vis system respectively. These properties were mainly affected by the topography of the material. Schwann cells attached strongly and proliferated on all the substrates.

The cell adhesion/orientation engineering profile is mainly affected by the topography, while the cell proliferation is influenced by the topography.

The specific cell patterning model involving anisotropic continuous microgrooves (PET-MG) and anisotropic discontinuous microspikes with parallel orientations (PLGA-MS replicas) were developed in an attempt to imitate native nerve regeneration-support structures and in particular imitating the guidance/alignment and growth of Schwann cells. It is known that primary Schwann cells transiently proliferate and form longitudinal bands of Bürger (boB) [53]. Aligned Schwann cells and their extracellular matrix are indispensable pathways for oriented axonal regrowth. The boB formation from a molecular point of view is unknown. A potential mechanism could be the polarized expression of adhesion proteins along the proximal-distal SC axis [53]. It was reported that placement of dissimilar adhesion characteristics in separate SC surface domains could aid longitudinal cell alignment. From a physical point of view, the basal lamina tube (enwrapping SCs and myelinated axons) is the guiding cue for axonal regrowth [53].

Two different "axonal guidance"' models were studied here. By using the same microfabrication techniques, two models were fabricated with different topographical (anisotropic continuous vs discontinuous) geometries. The same cell type was tested. Schwann cells adhered, grew, equally aligned and proliferated in both the models. Both models featuring topographical cues (pattern) with a combination of nano- and micro-characteristics are proposed to overcome the weaknesses of the existing and well-studied horizontal (grooves and ridges) or vertical (pillars, pores) cell patterning models.

The ability of this micropatterned strategy to control the cellular adhesion and growth and thus to engineer cell alignment *in vitro* could be potentially useful to a wide range of neuroscience subfields including basic research to understand cell interactions and network behavior, dynamic microenvironment systems that would better simulate the desired *in vivo* conditions and finally neural tissue engineering with the creation of implantable scaffolds for nerve tissue regeneration.

3. Materials and Methods

3.1 Experimental setup used for the fabrication of laser-microstructured substrates

The microstructured substrates have been prepared by ultrafast laser structuring, which is a simple but effective method to fabricate micro/nanostructures with different geometries [41]. The specially treated PET (polyethylene terephthalate) coverslips for cell culture were subjected to laser irradiation. A Yb:KGW laser was used with a pulse duration equal to 170 fs, 1 kHz repetition rate, and 1026 nm wavelength. The beam propagated through a half waveplate and a linear polarizer (which were used to vary the values of power), to a shutter (that was used to control the exposure time and thus the number of pulses receptive to the sample), then to a convex lens of 10 mm focal length and finally to the sample (Figure 7). The microstructured substrates were fabricated at a constant fluence of 11.9 J/cm^2, scan velocity of 7 mm/s and a x_{step} (distance between two consecutive scan lines) of 50 μm. The overall patterned area was 4mmx4mm.

Preprints (www.preprints.org) | NOT PEER-REVIEWED | Posted: 25 June 2018 doi:10.20944/preprints201806.0380.v1

Peer-reviewed version available at Int. J. Mol. Sci. 2018, 19, 2053; doi:10.3390/ijms19072053

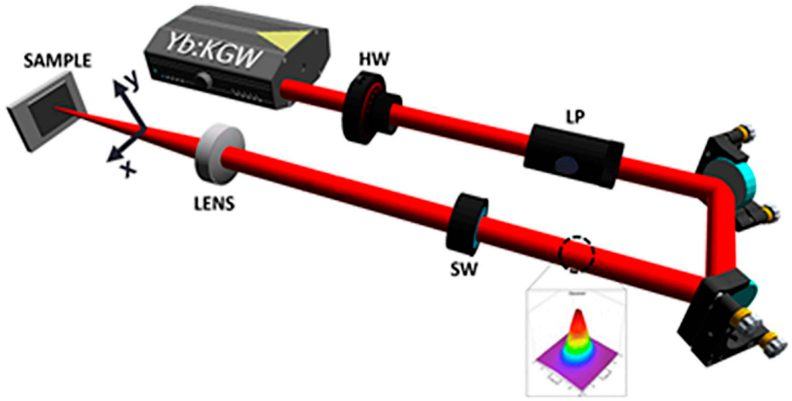

Figure 7. Experimental setup used for the fabrication of laser-microstructured substrates [42].

The same laser setup (Figure 7) was used to fabricate the Si substrates as described above. Single crystal n-type Silicon (1 0 0) wafers were subjected to laser irradiation in a vacuum chamber evacuated down to a residual pressure of 10^{-2} mbar. A constant sulfur hexafluoride (SF6) pressure of 650 mbar was maintained during the process through a precision microvalve system. A Yb:KGW laser was used with a pulse duration equal to 170 fs, 1 kHz repetition rate, and 1026 nm wavelength. The sample was mounted on a high-precision X–Y translation stage normal to the incident laser beam. The laser fluence used in these experiments was in the range (0.42 – 0.72 J/cm²), thus creating three different topographies defined as low, medium and high topography [20,21]. The overall spike area was 5mmx5mm. After laser irradiation, micro-structured surfaces were morphologically characterized by scanning electron microscopy (SEM). The top SEM images (d, e, f in Figure 1c) revealed an arbitrary shaped cross-section of the microstructures (MS) at low fluences that became almost elliptical as the laser fluence increased.

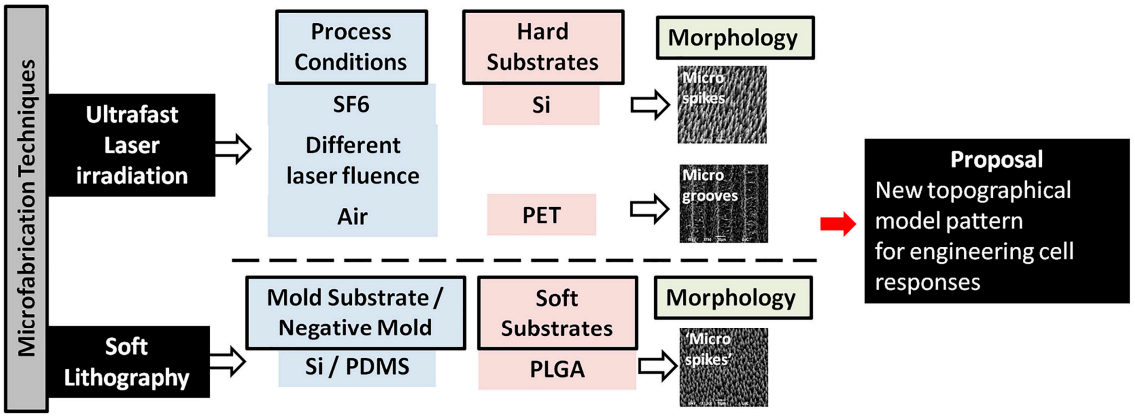

Laser Source	Wavelength (nm)	Pulse duration (fs)	Repetition Rate (kHz)	Sub-strate	Fluence (J/cm²)	Atmo-sphere	Structure	Geometry
Yb:KGW	1026	170	1	PET	11.9	Air	Microgrooves	Anisotropic Continuous
				Si	0.42-0.72	SF_6	Microspikes	Anisotropic Discontinuous

Figure 8. Comparison of the microfabricating techniques used in this study to fabricate the laser-microstructured substrates; the table demonstrates the conditions of the ultrafast laser irradiation process.

The laser-fabricated Si substrate is characterized as the "master" substrate. Negative replicas of the three master Si substrates were produced on elastomeric PDMS (SYLGARD 184, Dow Corning). In particular, liquid PDMS pre-polymer consisting of a "base" and "curing agent" typically mixed in a 10:1 w:w ratio was poured onto each substrate [54]. Then, the PDMS-coated Si substrates were placed into a vacuum chamber to remove residual air bubbles and thus providing a better penetration of the polymer into the laser-microstructures. After heating at 80 ◦C for 2 hours, a mold, which holds the negative of the original pattern, was peeled off of each Si substrate. An adequate number of PDMS negative molds was produced. Using the PDMS negative mold (negative spikes morphology), replicas of the initial morphology can be made out of several polymeric materials. In this study, we demonstrate the successful reproduction of the initial Si morphologies on PLGA replicas. A PLGA (Lactide:Glycolide 65:35, MW 40-75k) polymeric solution of 1:10 (Code No: P2066,Sigma Aldrich) in dichloromethane (DCM) was carefully prepared. The PLGA solution was magnetically stirred for 2 hours at room temperature (RT). One droplet of the PLGA solution was poured onto each PDMS negative mold and slowly finger-pressed with a glass disc. Following the evaporation of the solvent (24-48h in −20 ◦C) the PLGA-coated PDMS mold was placed in 4 ◦C for 2 hours. Then, the PLGA replica was peeled off the PDMS negative mold with a pair of tweezers.

3.2 Characterization of laser-microstructured substrates

3.2.1 Scanning Electron Microscopy (SEM)

The laser-microstructured substrates were morphologically characterized by Scanning Electron Microscopy (SEM) (JEOL JSM-6390 LV). Specifically, the substrates were sputter-coated with a 15 nm layer of gold (Baltec SCD 050) and observed under the microscope with an acceleration voltage of 15 kV. Fiji ImageJ, an image processing software, was used to perform the analysis of the geometrical characteristics of the microgrooves and microspikes on the three topographies, as described in [20,21]. Briefly, the aspect ratio of the microgrooves/microspikes, A, was calculated by dividing the depth/height of the microgrooves/microspikes over the width. The roughness ratio, r, was calculated by dividing the actual, unfolded surface area of microgrooves/microspikes over the total irradiated area.

For the determination of the directionality of the PLGA-MS replicas the "Local gradient orientation" for directionality was performed using the Fiji ImageJ plug-in "Directionality" [43].

3.2.2 Wettability measurements of laser-microstructured substrates

The contact angles of the laser-microstructured substrates were calculated via an automated tensionmeter, using the sessile drop method. A droplet of distilled, deionized Millipore water with volume 4 μL was positioned on the surface of the substrates, using a microsyringe, and images were taken to measure the angle formed at the liquid-solid interface.

3.2.3 UV-Vis measurements of laser-microstructured substrates

The UV-Vis absorption spectra of the laser-microstructured substrates were measured with a LAMBDA 950 UV/VIS/NIR spectrophotometer of Perkin Elmer with spectral range from 250 nm to 1200 nm. Laser-microstructured substrates and their relevant flat substrates were used for these measurements.

3.3 Cell culture

The Schwann (SW10) mouse cell line, is an established adherent neuronal Schwann cell line; immortalized with SV40 large T antigen. SW10 cells were obtained from ATCC® (Code:

CRL-2766™). Schwann cells were grown in cell culture flasks using Dulbecco's modified Eagle's medium [DMEM (Invitrogen, Grand Island, NY, USA) supplemented with 10% fetal bovine serum (Biosera, Sussex, UK)] in a 5% CO2 incubator (Thermo Scientific) at 33 °C. Laser-microstructured substrates were UV sterilized and transferred into sterile wells of 24 well plates (Sarstedt; Numbrecht, Germany). $3x10^4$ cells in culture medium were seeded on the substrates and were cultured for a series of different time periods depending on the substrates, ranging from three to six days. The cell orientation and proliferation were better assessed for four and six days for the PET substrates, while for the PLGA replicas the optimized time points are three and five days. The control samples in all the experiments were PET (polyethylene terephthalate) coverslips for cell culture.

3.3.1 Morphology of Schwann (SW10) cells by Scanning Electron Microscopy (SEM)

The laser-microstructured substrates seeded with the SW10 cells were removed from the incubator, washed twice with 0.1 M sodium cacodylate buffer (SCB) and fixed with 2% glutaraldehyde (GDA) and 2% paraformaldehyde (PFA) in 0.1 M SCB for 30 minutes. Thereafter, they were washed twice with 0.1 M SCB and dehydrated in increasing concentrations (from 30-100%) of ethanol. Finally, they were dried in a critical point drier (Baltec CPD 030), sputter-coated with a 15 nm layer of gold (Baltec SCD 050) and observed under a Scanning Electron Microscope (JEOL JSM-6390 LV) at an accelerating voltage of 15 kV. For the PLGA replicas, CPD cannot be used since it deforms the polymer, so after an optimization process, an hexamethyldisilizane (HDMS) protocol was established. After the dehydration steps with ethanol (EtOH), EtOH: HDMS solutions (50:50) were used for specific time points to all the replicas and then the same procedure was repeated with HDMS solutions. Finally, the replicas were left to dry at room temperature overnight.

To investigate changes in directional orientation of Schwann cells on the microstructured substrates the "Local gradient orientation" for directionality was performed using the Fiji ImageJ plug-in "Directionality" [43].

3.3.2 Immunocytochemical assay

SW10 cells were stained for F-actin. Specifically, after four and six days of culture, the samples were fixed with 4% PFA for 15 minutes and permeabilized with 0.1% Triton X-100 in PBS for 5 minutes. The non-specific binding sites were blocked with 2% BSA in PBS for 30 minutes. Then, the samples were incubated for 2 hours at room temperature with Alexa Fluor® 568 Phalloidin (Invitrogen-Thermo Fisher Scientific) (1:250 in PBS–BSA 1%) for F-actin staining. Finally, the samples were washed with PBS and put on coverslips with DAPI (Molecular probes by Life Technologies) for nuclei staining. Cell imaging was performed using an epifluorescence microscope coupled to a high-resolution Carl Zeiss Axiocam color camera. The objectives of x10 and x20 were used. The number of SW10 cells that have been grown on the microstructured substrates were determined by counting cell nuclei stained with DAPI. Nuclei number was assessed with Image J (cell counter plugin). The results represent the means of three different experiments (n=10 fields of view-images for each substrate and time point).

3.3.3 Live dead Assay

SW10 cells were seeded onto a PLGA replica to a density of $3x10^4$ cells/well. After three and five days, incubation under standardized culture conditions medium was removed and replaced a live/dead viability/cytotoxicity kit. The LIVE/DEAD™ Viability/Cytotoxicity Kit, for mammalian cells (L3224, Thermo Scientific) was used for valuing the cell viability and proliferation. The cell-adhered replicas were washed twice with PBS. A live/dead solution was prepared by adding 20μL of the supplied 2mM ethidium homodimer-1 (EthD-1) stock solution to 10 mL of sterile PBS (thus reaching the desired concentration of 4μM EthD-1 solution) and after mixing thoroughly, added 5μL of the supplied 4 mM calcein AM stock solution to the 10 mL EthD-1 solution (thus reaching the desired concentration of 2μM calcein AM solution). The solution was directly added to

the replicas in order to cover the whole sample and was left for 45 min at room temperature. Finally, the cells were washed once with PBS and fluorescent images were obtained by the fluorescent microscope (images not shown here). The number of SW10 cells that have been grown on the microstructured substrates were determined by counting cell nuclei stained with calcein. Nuclei number was assessed with Image J (cell counter plugin). The results represent the means of three different experiments (n=10 fields of view-images for each substrate and time point).

3.4 Statistical Analysis

The data were subjected to ANOVA with post-hoc Tukey HSD Test to compare the significance levels ($p<0.05$) between multiple groups.

4. Conclusions

A successful fabrication of the micropatterned substrates was accomplished via ultrafast laser irradiation and soft lithography. Ultrafast-pulsed laser irradiation is a simple and effective method to fabricate micro- and nano-structures with controlled geometry and pattern regularity. The anisotropic continuous (PET-MG) and discontinuous (PLGA-MS replicas) microstructured polymeric substrates were assessed in terms of their geometrical-topographical parameters (aspect ratio, roughness and directionality) and their influence and reproducibility on the Schwann cells responses. The cells attached strongly and proliferated well on the substrates. Surface topography affected Schwann cells. Moreover, cells appeared to be oriented along the direction of the microgrooves and microspikes. This micropatterned strategy to control the cellular adhesion and growth and thus to engineer cell alignment *in vitro* could be potentially useful in the field of neural tissue engineering and for the assessment in dynamic microenvironments simulating more sufficient the *in vivo* conditions.

Acknowledgments: This work was supported from funding by NFFA (EU H2020 framework programme) under grant agreement n. 654360 from 1/9/2015 to 31/8/2019, State Scholarship Foundation (IKY) within the framework of the Action "Doctoral Research Support" (MIS 5000432), ESPA 2014-2020 Program, CN: 2016-ESPA-050-0502-5321 and Onassis Foundation through the G ZM 039-1/2016-2017 scholarship grant. We acknowledge also support of this work by the project "Advanced Research Activities in Biomedical and Agro alimentary Technologies" (MIS 5002469) which is implemented under the "Action for the Strategic Development on the Research and Technological Sector", funded by the Operational Programme "Competitiveness, Entrepreneurship and Innovation" (NSRF 2014-2020) and co-financed by Greece and the European Union (European Regional Development Fund).

Author Contributions: Eleftheria Babaliari performed the full study of the PET microstructured substrates (from their fabrication, characterization of their properties, cell studies and analyzing the data); Paraskevi Kavatzikidou performed the PLGA replicas and their assessment (from their replication, characterization, cell studies and analyzing the data); Despoina Angelaki performed the fabrication of the Si microstructured substrates used for the PLGA replication; Lefki Chaniotaki performed the characterization of the PLGA replicas in terms of morphology, contact angle measurements and optical properties; Alexandra Manousaki performed all the SEM imaging; Alexandra Siakouli-Galanopoulou optimized the HDMS protocol for the successful preparation of the PLGA replicas for SEM imaging and performed some of the SEM imaging on PLGA replicas with SW10 cells; Anthi Ranella contributed to the study objectives, supervision and writing of paper; Emmanuel Stratakis contributed with funding this study, supervision, and writing of paper.

Conflicts of Interest: The authors declare no conflict of interest.

583 **Abbreviations**

584

2D	Two-dimensional
A	Absorbance
ATR-FTIR	Attenuated Total Reflection-Fourier Transform Infrared (spectroscopy)
BSA	Bovine Serum Albumen
CO_2	Carbon dioxide
CPD	Critical Point Dryer
DAPI	4',6-Diamidino-2-Phenylindole
DCM	Dichloromethane
DMEM	Dulbecco's Modified Eagles Medium
ECM	Extracellular matrix
EthD-1	Ethidium Homodimer-1
EtOH	Ethanol
GDA	Glutaraldehyde
HDMS	Hexamethyldisilizane
IESL	Institute of Electronic Structure and Laser
MG	Microgrooves
MS	Microspikes
NGF	Nerve Growth Factor
PBS	Phosphate-buffered saline
PC12	Pheochromocytoma
PDMS	Poly(dimethylsiloxane)
PET	Polyethylene terephthalate
PFA	Paraformaldehyde
PLGA	Poly(lactide-co-glycolide)
RT	Room Temperature
SCB	Sodium Cacodylate buffer
SEM	Scanning Electron Microscopy
SF_6	Sulfur hexafluoride
Si	Silicon
SW10	Schwann cells
UV	Ultraviolet
UV-Vis	Ultraviolet-Visible
UV/VIS/NIR	Ultraviolet/Visible/Near Infrared
Yb:KGW	Ytterbium-doped potassium gadolinium tungstate

585 **References**

586 1. Wu, R.-X.; Yin, Y.; He, X.-T.; Li, X.; Chen, F.-M. Engineering a Cell Home for Stem Cell Homing and
587 Accommodation. *Adv. Biosyst.* **2017**, *1*, 1700004, doi:10.1002/adbi.201700004.

588 2. Stevens, M. M.; George, J. H. Exploring and Engineering the Cell Surface Interface. *Science (80-.).* **2005**,
589 *310*, 1135–1138, doi:10.1126/science.1106587.

590 3. Pasapera, A. M.; Schneider, I. C.; Rericha, E.; Schlaepfer, D. D.; Waterman, C. M. Myosin II activity
591 regulates vinculin recruitment to focal adhesions through FAK-mediated paxillin phosphorylation. *J.*
592 *Cell Biol.* **2010**, *188*, 877–90, doi:10.1083/jcb.200906012.

4. Crowder, S. W.; Leonardo, V.; Whittaker, T.; Papathanasiou, P.; Stevens, M. M. Material Cues as Potent Regulators of Epigenetics and Stem Cell Function. *Cell Stem Cell* **2016**, *18*, 39–52, doi:10.1016/J.STEM.2015.12.012.

5. Dalby, M. J.; Gadegaard, N.; Oreffo, R. O. C. Harnessing nanotopography and integrin–matrix interactions to influence stem cell fate. *Nat. Mater.* **2014**, *13*, 558–569, doi:10.1038/nmat3980.

6. Stukel, J. M.; Willits, R. K. Mechanotransduction of Neural Cells Through Cell–Substrate Interactions. *Tissue Eng. Part B Rev.* **2016**, *22*, 173–182, doi:10.1089/ten.teb.2015.0380.

7. Yiannakou, C.; Simitzi, C.; Manousaki, A.; Fotakis, C.; Ranella, A.; Stratakis, E. Cell patterning via laser micro/nano structured silicon surfaces. *Biofabrication* **2017**, *9*, 25024, doi:10.1088/1758-5090/aa71c6.

8. Wang, X.; Ohlin, C. A.; Lu, Q.; Hu, J. Cell directional migration and oriented division on three-dimensional laser-induced periodic surface structures on polystyrene. *Biomaterials* **2008**, *29*, 2049–2059, doi:10.1016/j.biomaterials.2007.12.047.

9. Rebollar, E.; Frischauf, I.; Olbrich, M.; Peterbauer, T.; Hering, S.; Preiner, J.; Hinterdorfer, P.; Romanin, C.; Heitz, J. Proliferation of aligned mammalian cells on laser-nanostructured polystyrene. *Biomaterials* **2008**, *29*, 1796–1806, doi:10.1016/J.BIOMATERIALS.2007.12.039.

10. Ranella, A.; Barberoglou, M.; Bakogianni, S.; Fotakis, C.; Stratakis, E. Tuning cell adhesion by controlling the roughness and wettability of 3D micro/nano silicon structures. *Acta Biomater.* **2010**, *6*, 2711–2720, doi:10.1016/J.ACTBIO.2010.01.016.

11. Orgovan, N.; Peter, B.; Bősze, S.; Ramsden, J. J.; Szabó, B.; Horvath, R. Dependence of cancer cell adhesion kinetics on integrin ligand surface density measured by a high-throughput label-free resonant waveguide grating biosensor. *Sci. Rep.* **2015**, *4*, 4034, doi:10.1038/srep04034.

12. Makarona, E.; Peter, B.; Szekacs, I.; Tsamis, C.; Horvath, R. ZnO Nanostructure Templates as a Cost-Efficient Mass-Producible Route for the Development of Cellular Networks. *Materials (Basel).* **2016**, *9*, 256, doi:10.3390/ma9040256.

13. Simitzi, C.; Karali, K.; Ranella, A.; Stratakis, E. Controlling the Outgrowth and Functions of Neural Stem Cells: The Effect of Surface Topography. *ChemPhysChem* **2018**, doi:10.1002/cphc.201701175.

14. Simitzi, C.; Ranella, A.; Stratakis, E. Controlling the morphology and outgrowth of nerve and neuroglial cells: The effect of surface topography. *Acta Biomater.* **2017**, *51*, 21–52, doi:10.1016/J.ACTBIO.2017.01.023.

15. Abdeen, A. A.; Lee, J.; Kilian, K. A. Capturing extracellular matrix properties in vitro: Microengineering materials to decipher cell and tissue level processes. *Exp. Biol. Med.* **2016**, *241*, 930–938, doi:10.1177/1535370216644532.

16. Chen, W.; Shao, Y.; Li, X.; Zhao, G.; Fu, J. Nanotopographical surfaces for stem cell fate control: Engineering mechanobiology from the bottom. *Nano Today* **2014**, *9*, 759–784, doi:10.1016/J.NANTOD.2014.12.002.

17. Griffith, L. G.; Swartz, M. A. Capturing complex 3D tissue physiology in vitro. *Nat. Rev. Mol. Cell Biol.* **2006**, *7*, 211–224, doi:10.1038/nrm1858.

18. Mirzadeh, H.; Dadsetan, M. Influence of laser surface modifying of polyethylene terephthalate on fibroblast cell adhesion. *Radiat. Phys. Chem.* **2003**, *67*, 381–385, doi:10.1016/S0969-806X(03)00071-9.

19. Dadsetan, M.; Mirzadeh, H.; Sharifi-Sanjani, N.; Salehian, P. IR LASER SURFACE MODIFICATION OF POLYETHYLENE TEREPHTHALATE AS BIOMATERIAL. In *Processing and Fabrication of Advanced Materials VIII*; WORLD SCIENTIFIC, 2001; pp. 221–229.

20. Simitzi, C.; Efstathopoulos, P.; Kourgiantaki, A.; Ranella, A.; Charalampopoulos, I.; Fotakis, C.; Athanassakis, I.; Stratakis, E.; Gravanis, A. Laser fabricated discontinuous anisotropic microconical substrates as a new model scaffold to control the directionality of neuronal network outgrowth. *Biomaterials* **2015**, *67*, 115–128, doi:10.1016/j.biomaterials.2015.07.008.

21. Simitzi, C.; Stratakis, E.; Fotakis, C.; Athanassakis, I.; Ranella, A. Microconical silicon structures influence NGF-induced PC12 cell morphology. *J. Tissue Eng. Regen. Med.* **2015**, *9*, 424–434, doi:10.1002/term.1853.

22. Stratakis, E.; Ranella, A.; Fotakis, C. Biomimetic micro/nanostructured functional surfaces for microfluidic and tissue engineering applications. *Biomicrofluidics* **2011**, *5*, 13411, doi:10.1063/1.3553235.

23. Chow, W. N.; Simpson, D. G.; Bigbee, J. W.; Colello, R. J. Evaluating neuronal and glial growth on electrospun polarized matrices: bridging the gap in percussive spinal cord injuries. *Neuron Glia Biol.* **2007**, *3*, 119–26, doi:10.1017/S1740925X07000580.

24. Schnell, E.; Klinkhammer, K.; Balzer, S.; Brook, G.; Klee, D.; Dalton, P.; Mey, J. Guidance of glial cell migration and axonal growth on electrospun nanofibers of poly-ε-caprolactone and a collagen/poly-ε-caprolactone blend. *Biomaterials* **2007**, *28*, 3012–3025, doi:10.1016/J.BIOMATERIALS.2007.03.009.

25. Hoffman-Kim, D.; Mitchel, J. A.; Bellamkonda, R. V Topography, cell response, and nerve regeneration. *Annu. Rev. Biomed. Eng.* **2010**, *12*, 203–31, doi:10.1146/annurev-bioeng-070909-105351.

26. Johansson, F.; Carlberg, P.; Danielsen, N.; Montelius, L.; Kanje, M. Axonal outgrowth on nano-imprinted patterns. *Biomaterials* **2006**, *27*, 1251–1258, doi:10.1016/J.BIOMATERIALS.2005.07.047.

27. Yao, L.; Wang, S.; Cui, W.; Sherlock, R.; O 'connell, C.; Damodaran, G.; Gorman, A.; Windebank, A.; Pandit, A. Effect of functionalized micropatterned PLGA on guided neurite growth. **2008**, doi:10.1016/j.actbio.2008.09.002.

28. Schulte, C.; Rodighiero, S.; Cappelluti, M. A.; Puricelli, L.; Maffioli, E.; Borghi, F.; Negri, A.; Sogne, E.; Galluzzi, M.; Piazzoni, C.; Tamplenizza, M.; Podestà, A.; Tedeschi, G.; Lenardi, C.; Milani, P. Conversion of nanoscale topographical information of cluster-assembled zirconia surfaces into mechanotransductive events promotes neuronal differentiation. *J. Nanobiotechnology* **2016**, *14*, 18, doi:10.1186/s12951-016-0171-3.

29. Maffioli, E.; Schulte, C.; Nonnis, S.; Grassi Scalvini, F.; Piazzoni, C.; Lenardi, C.; Negri, A.; Milani, P.; Tedeschi, G. Proteomic Dissection of Nanotopography-Sensitive Mechanotransductive Signaling Hubs that Foster Neuronal Differentiation in PC12 Cells. *Front. Cell. Neurosci.* **2018**, *11*, 417, doi:10.3389/fncel.2017.00417.

30. Schulte, C.; Ripamonti, M.; Maffioli, E.; Cappelluti, M. A.; Nonnis, S.; Puricelli, L.; Lamanna, J.; Piazzoni, C.; Podestà, A.; Lenardi, C.; Tedeschi, G.; Malgaroli, A.; Milani, P. Scale Invariant Disordered Nanotopography Promotes Hippocampal Neuron Development and Maturation with Involvement of Mechanotransductive Pathways. *Front. Cell. Neurosci.* **2016**, *10*, 267, doi:10.3389/fncel.2016.00267.

31. Zerva, I.; Simitzi, C.; Siakouli-Galanopoulou, A.; Ranella, A.; Stratakis, E.; Fotakis, C.; Athanassakis, I. Implantable vaccine development using in vitro antigen-pulsed macrophages absorbed on laser micro-structured Si scaffolds. *Vaccine* **2015**, *33*, 3142–3149, doi:10.1016/J.VACCINE.2015.04.017.

32. Geissler, M.; Xia, Y. Patterning: Principles and Some New Developments. *Adv. Mater.* **2004**, *16*, 1249–1269, doi:10.1002/adma.200400835.

33. Whitesides, G. M. The origins and the future of microfluidics. *Nature* **2006**, *442*, 368–373, doi:10.1038/nature05058.

34. Nikkhah, M.; Edalat, F.; Manoucheri, S.; Khademhosseini, A. Engineering microscale topographies to control the cell–substrate interface. *Biomaterials* **2012**, *33*, 5230–5246, doi:10.1016/J.BIOMATERIALS.2012.03.079.

35. Chollet, C.; Chanseau, C.; Remy, M.; Guignandon, A.; Bareille, R.; Labrugère, C.; Bordenave, L.; Durrieu, M.-C. The effect of RGD density on osteoblast and endothelial cell behavior on RGD-grafted polyethylene terephthalate surfaces. *Biomaterials* **2009**, *30*, 711–720, doi:10.1016/j.biomaterials.2008.10.033.

36. Li, Y.; Ma, T.; Yang, S.-T.; Kniss, D. A.; Kniss, D. A. Thermal compression and characterization of three-dimensional nonwoven PET matrices as tissue engineering scaffolds. *Biomaterials* **2001**, *22*, 609–618, doi:10.1016/S0142-9612(00)00224-6.

37. Lima, M. J.; Correlo, V. M.; Reis, R. L. Micro/nano replication and 3D assembling techniques for scaffold fabrication. *Mater. Sci. Eng. C* **2014**, *42*, 615–621, doi:10.1016/J.MSEC.2014.05.064.

38. Qian, L.; Ahmed, A.; Glennon-Alty, L.; Yang, Y.; Murray, P.; Zhang, H. Patterned substrates fabricated by a controlled freezing approach and biocompatibility evaluation by stem cells. *Mater. Sci. Eng. C* **2015**, *49*, 390–399, doi:10.1016/J.MSEC.2015.01.034.

39. Tay, C.; Pal, M.; Yu, H.; Leong, W.; Tan, N.; Small, K. N.-; 2011, undefined Bio-inspired Micropatterned Platform to Steer Stem Cell Differentiation. *Wiley Online Libr.*

40. Mandoli, C.; Pagliari, F.; Pagliari, S.; Forte, G.; Di Nardo, P.; Licoccia, S.; Traversa, E. Stem Cell Aligned Growth Induced by CeO2 Nanoparticles in PLGA Scaffolds with Improved Bioactivity for Regenerative Medicine. *Adv. Funct. Mater.* **2010**, *20*, 1617–1624, doi:10.1002/adfm.200902363.

41. Stratakis, E.; Ranella, A.; Fotakis, C. Laser-Based Biomimetic Tissue Engineering. In; Springer, Berlin, Heidelberg, 2013; pp. 211–236.

42. Skoulas, E.; Manousaki, A.; Fotakis, C.; Stratakis, E. Biomimetic surface structuring using cylindrical vector femtosecond laser beams. *Sci. Rep.* **2017**, *7*, 45114, doi:10.1038/srep45114.

43. Schindelin, J.; Arganda-Carreras, I.; Frise, E.; Kaynig, V.; Longair, M.; Pietzsch, T.; Preibisch, S.; Rueden, C.; Saalfeld, S.; Schmid, B.; Tinevez, J.-Y.; White, D. J.; Hartenstein, V.; Eliceiri, K.; Tomancak, P.; Cardona, A. Fiji: an open-source platform for biological-image analysis. *Nat. Methods* **2012**, *9*, 676–82, doi:10.1038/nmeth.2019.

44. Donelli, I.; Taddei, P.; Smet, P. F.; Poelman, D.; Nierstrasz, V. A.; Freddi, G. Enzymatic surface modification and functionalization of PET: A water contact angle, FTIR, and fluorescence spectroscopy study. *Biotechnol. Bioeng.* **2009**, *103*, 845–856, doi:10.1002/bit.22316.

45. Zorba, V.; Stratakis, E.; Barberoglou, M.; Spanakis, E.; Tzanetakis, P.; Anastasiadis, S. H.; Fotakis, C. Biomimetic Artificial Surfaces Quantitatively Reproduce the Water Repellency of a Lotus Leaf. *Adv. Mater.* **2008**, *20*, 4049–4054, doi:10.1002/adma.200800651.

46. D 'avila, C.; Erbetta, C.; Alves, R. J.; Resende, J. M.; Fernando De Souza Freitas, R.; Geraldo De Sousa, R. Synthesis and Characterization of Poly(D,L-Lactide-co-Glycolide) Copolymer. *J. Biomater. Nanobiotechnol.* **2012**, *3*, 208–225, doi:10.4236/jbnb.2012.32027.

47. Grossetête, T.; Rivaton, A.; Gardette, J. L.; Hoyle, C. E.; Ziemer, M.; Fagerburg, D. R.; Clauberg, H. Photochemical degradation of poly(ethylene terephthalate)-modified copolymer. *Polymer (Guildf).* **2000**, *41*, 3541–3554, doi:10.1016/S0032-3861(99)00580-7.

48. Fechine, G. J. .; Rabello, M. S.; Souto Maior, R. M.; Catalani, L. H. Surface characterization of photodegraded poly(ethylene terephthalate). The effect of ultraviolet absorbers. *Polymer (Guildf).* **2004**, *45*, 2303–2308, doi:10.1016/J.POLYMER.2004.02.003.

49. Prasad, S. G.; De, A.; De, U. Structural and Optical Investigations of Radiation Damage in Transparent PET Polymer Films. *Int. J. Spectrosc.* **2011**, *2011*, 1–7, doi:10.1155/2011/810936.

50. Upson, S. J.; Partridge, S. W.; Tcacencu, I.; Fulton, D. A.; Corbett, I.; German, M. J.; Dalgarno, K. W. Development of a methacrylate-terminated PLGA copolymer for potential use in craniomaxillofacial fracture plates. *Mater. Sci. Eng. C* **2016**, *69*, 470–477, doi:10.1016/J.MSEC.2016.06.012.

51. Qi, L.; Li, N.; Huang, R.; Song, Q.; Wang, L.; Zhang, Q.; Su, R.; Kong, T.; Tang, M.; Cheng, G. The Effects of Topographical Patterns and Sizes on Neural Stem Cell Behavior. *PLoS One* **2013**, *8*, e59022, doi:10.1371/journal.pone.0059022.

52. Serrano, M. C.; Chung, E. J.; Ameer, G. A. Advances and Applications of Biodegradable Elastomers in Regenerative Medicine. *Adv. Funct. Mater.* **2010**, *20*, 192–208, doi:10.1002/adfm.200901040.

53. Lietz, M.; Dreesmann, L.; Hoss, M.; Oberhoffner, S.; Schlosshauer, B. Neuro tissue engineering of glial nerve guides and the impact of different cell types. *Biomaterials* **2006**, *27*, 1425–1436,

732 doi:10.1016/J.BIOMATERIALS.2005.08.007.

733 54. Koufaki, N.; Ranella, A.; Aifantis, K. E.; Barberoglou, M.; Psycharakis, S.; Fotakis, C.; Stratakis, E.
734 Controlling cell adhesion via replication of laser micro/nano-textured surfaces on polymers.
735 *Biofabrication* **2011**, *3*, 45004, doi:10.1088/1758-5082/3/4/045004.